The solar-wind driven magnetosphere–ionosphere as a complex dynamical system

W. Horton, J. P. Smith, R. Weigel, and C. Crabtree
Institute for Fusion Studies, The University of Texas at Austin, Austin, Texas 78712

I. Doxas, B. Goode, and J. Cary
Department of Physics, University of Colorado, Boulder, Colorado 80309-0390

(Received 19 April 1999; accepted 12 June 1999)

The solar-wind driven magnetosphere–ionosphere system is a classic example of a complex dynamical system (CDS). The defining properties of a CDS are (1) sensitivity to initial conditions; (2) multiple space-time scales; (3) bifurcation sequences with hysteresis in transitions between attractors; and (4) noncompositionality. Noncompositionality means that the behavior of the system as a whole is different from the dynamics of its subcomponents taken with passive or no couplings. In particular the dynamics of the geomagnetic tail plasma depends on its coupling to the dissipative ionospheric plasma and on the nature of the solar-wind driving electric field over a suitably long (many hours) previous time interval. These complex dynamical system features are shown here in detail using the known WINDMI model for the solar-wind driven magnetosphere–ionosphere (MI) system. Numerous features in the bifurcation sequence are identified with known substorm and storm characteristics. © *1999 American Institute of Physics*. [S1070-664X(99)03111-0]

I. INTRODUCTION

Physical systems often exhibit a surprising variety of complex dynamical forms for relatively small changes in either the external forcing conditions or the internal parameters of the system. The new science of *chaos*[1] is able to explain why such rich, complex behavior is universal in many physical systems with sufficient complexity. These systems are often called complex dynamical systems (CDS) with properties defined below. The quantitative explanation of such behavior can often be expressed in terms of low-dimensional dynamical models even though there are many degrees of freedom ($N \gg 10^6$) in the traditional microscopic physical modeling. This reduction to low-dimensional behavior occurs due to the strong phase space contraction associated with volumes defined by arbitrary clouds of initial datapoints $\mathbf{Z}_i(t_0)$ in the full, high-dimensional $\mathbb{R}^{2N}$ phase space. The cloud contracts to a submanifold of dimension d that is sufficient to describe the dominant dynamical components. The submanifold can be described by a few key physical variables typically defined by the major energy components of the system. For the solar-*wind* driven *magnetosphere–ionosphere* system, the WINDMI model[2–4] is a $d=6$ principal energy component low-dimensional model. The derivation of the model is given in Refs. 4 and 5. The performance of the model has been tested on the one 40 h interval (interval 20) of the Bargatze *et al*.[6] substorm database and for the January 14–15, 1988 magnetic cloud event described by Ref. 7 and reproduced in Ref. 4 with WINDMI. Here we will show the performance on a high activity level interval (30) of the Bargatze *et al*. database.

First we will display an example of the bifurcation sequences that occurs in the average cross-tail electric field response to a steady applied interplanetary magnetic field (IMF) electric field of increasing strength. The role of the solar-wind fluctuations is briefly discussed and the low-pass filter action of the MI system is noted as in Ref. 8. Fluctuations in the solar-wind driver down to 2.5 min are included from the IMP-8 database used in the Bargatze *et al*. database.

As with concepts of *turbulence* and *coherent structures*, the complex dynamical system is defined operationally by its key properties:

(1) sensitivity to initial conditions;

(2) multiple space–time scales;

(3) bifurcation sequences with hysteresis in the transitions between attractors;

(4) noncompositionality.

Here noncompositionality means that behavior of the system as a whole is different from the dynamics that would be inferred from the study of the dynamics of its subcomponents taken with passive or no couplings between the subcomponents. We define a CDS to be a system with all four properties. It appears that most driven dissipative systems with two of the properties will have all four.

Returning to the issue of low-dimensional behavior, it should be recognized that the conditions under which a physical system with many degrees of freedom will yield to such a reduced dynamical descriptions is not well understood. One theoretical model for the locking of many degrees of freedom is the self-organized criticality model.[9] Self-organization itself plays an important role in forming coherent structures. The modified Harris sheet of distributed plasma currents and pressures is a nonlinear self-consistent-field state on which some of the original WINDMI model calculations are based.[2]

In Sec. II we describe the WINDMI model and its properties. We discuss the earlier and current research on determining the dimension of the geomagnetic indices that measure the ionospheric currents at auroral latitudes, which is an

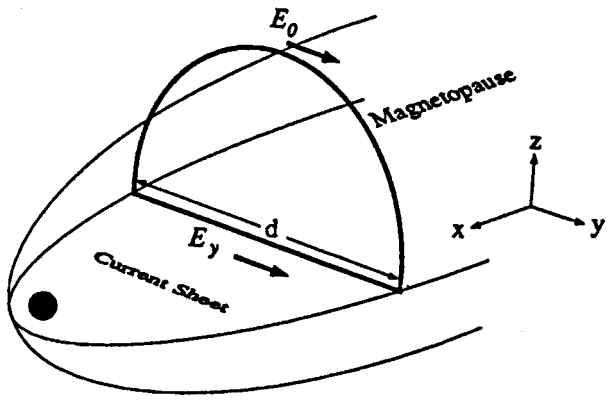

FIG. 1. Faraday loop [courtesy of Klimas *et al*. (1992)] taken from the model of the dripping faucet analog of substorms. The northern lobe magnetic flux $\int_{\text{lobe}}\mathbf{B}\cdot da = LI$ where $L \simeq 27-30$ H and the cross-tail current closing around the northern lobe is $I \simeq 2\times 10^7$ A. Detailed calculations of L and I from the Tsyganenko–Stern (1996) (Ref. 30) magnetosphere model are given in Ref. 4.

output of the WINDMI model. We describe the bifurcation sequence predicted by WINDMI which shows a progression of states from quiet time, to isolated substorms of increasing intensity to a final high level of steady unloading. We hypothesize that the final state is that of a magnetic storm and discuss those properties of storms[10] consistent with this interpretation. In Sec. III we discuss the dimensionality of the lower envelope of the auroral index (AL) index and the influence of the solar wind and noise. In Sec. IV we show the performance of the WINDMI model for one of the high level intervals (30) in the Bargatze dataset. In Sec. V we give the conclusions and note problems requiring further investigation.

II. THE WINDMI MODEL

The core mathematical structure of the WINDMI model is derived from that of a three-degree of freedom Hamiltonian system in the absence of driving and damping and for a perfectly reflecting closed box in $\mathbb{R}^3$. Including the physics that the magnetosphere–ionosphere is an open system (box) with a driven–damped plasma yields the final dissipative WINDMI system. Nonetheless, important constraints on the structure of the equations are obtained by considering the ideal limit. The ideal limit[11] shows that the natural pairs of variables are (I,V), $(P,K_\parallel)$, (I_1,V_i). Here the state is given by the geotail current $I(t)$ and cross-tail convection potential drop $V(t)=E_y(t)L_y$ following Ref. 12; the central plasma sheet pressure $P(t)$ and the parallel flow velocities $v_\parallel = \pm(2K_\parallel(t)/\rho_m\Omega)^{1/2}$. Here P is the mean plasma pressure, ρ_m is the mean mass density, and $K_\parallel$ the total parallel kinetic energy in the volume Ω of the central plasma sheet (CPS). The average ion mass m_p is taken as the proton mass. Figure 1 shows the Faraday loop used here and introduced in Ref. 12 to obtain the dynamical equation for the geotail current, $I(t)$.

The nightside region-1 current loop $I_1(t)$ and nightside ionospheric potential difference $V_i(t)$ associated with the footpoints of the substorm current wedge together with the cross-tail current loop (I,V) form a two-degree of freedom Hamiltonian system. The coupling is through the mutual inductance M of the linked magnetic fluxes. The two normal modes of the system[2,3] are the global geotail Alfvén oscillation ($T\sim 1$ h), and the $M-I$ coupling Alfvén wave ($T\sim 10$ min). The third timescale is associated with the loading and unloading of the CPS pressure. The high beta magnetoacoustic wave in the CPS with ($T\sim 1$ min) leads to incompressible flows on the time scale analyzed here. Imposing the condition of incompressible flows eliminates the sub-minute time scale variation. The nonlinear dynamics of the state vector $\mathbf{X}(t)=(I,V,P,K_\parallel,I_1,V_i)$ driven by the solar wind, $V_{\text{sw}}(t)=\beta E_y(t)$, with set of physical parameters $\{\mu\}_{i=1}^{15}=\{L,C,\Sigma,M,L_1,C_i,u_0,I_c,\Delta I,\tau_\parallel,\alpha,\Omega,\Sigma_i,\Sigma^{nl},\beta\}$ arises from the geometry and magnetic field of the planet, the characteristics of the two major current loops and the ionosphere. A complete definition of the parameters is given in Refs. 3 and 2.

The solar wind forcing $\mathbf{f}_{\text{sw}}(t)$ function has a regular coherent component $\langle V_{\text{sw}}(t)\rangle$ which is the particularly dangerous feature arising, for example, from coronal mass ejection forming large helical flux ropes. The predictions of WINDMI for the Farrugia *et al*.[7] 30 h magnetic cloud event is given by Ref. 4.

In addition there is a broad-band turbulent spectrum of the solar wind.[13] Thus, we have the stochastic differential equations

$$\frac{d\mathbf{X}}{dt} = L\mathbf{X} + \mathbf{f}^{nl}(\mathbf{X}) + \mathbf{f}_{\text{sw}}(t) \tag{1}$$

with the volume contracting flow

$$\sum_{i=1}^{6}\frac{\partial}{\partial X_i}\left(\frac{dX_i}{dt}\right) = -\Sigma - \frac{1}{\tau_E} - \frac{1}{\tau_\parallel} - \frac{\partial}{\partial V_i}(\Sigma_i V_i) < 0 \tag{2}$$

in the phase space. Thus an arbitrary initial volume in the full phase space contracts to a lower-dimensional subspace. The system attempts to evolve to fixed points where $L\mathbf{X}+\mathbf{f}^{nl}(\mathbf{X})+\mathbf{f}_{\text{sw}}=0$, but is always being kicked away from the fixed points by the solar-wind fluctuations. The fluctuation dissipation theorem[14] tells us the relationship between the variance $\langle \delta X^2\rangle$ and the fluctuation $\langle \delta \mathbf{f}_{\text{sw}}^2\rangle$.

The properties of the mode-coupling elements in Eq. (1) are best illustrated by going directly to the quadratic energy component equations:

$$\frac{d}{dt}\left(\frac{1}{2}LI^2\right) = \frac{LL_1}{L_1L-M^2}(V_{\text{sw}}-V)I + \frac{LM}{L_1L-M^2}(V-V_i)I, \tag{3}$$

$$\frac{d}{dt}\left(\frac{1}{2}CV^2\right) = IV - I_1V - \alpha P^{1/2}V - \Sigma V^2, \tag{4}$$

$$\frac{d}{dt}\left(\frac{3}{2}\Omega P\right) = \Sigma V^2 - u_0\Omega K_\parallel^{1/2}P\frac{1}{2}\left[1+\tanh\left(\frac{I-I_c}{\Delta I}\right)\right], \tag{5}$$

$$\frac{dK_\parallel}{dt} = \alpha P^{1/2}V - \frac{K_\parallel}{\tau_\parallel}, \tag{6}$$

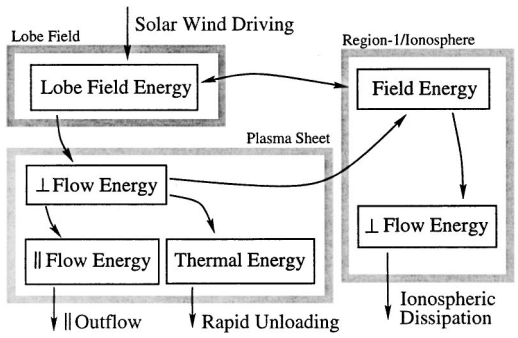

FIG. 2. Energy flow paths from the solar-wind dynamo during the lobe magnetic field storage and the subsequent flows paths out of the nightside magnetosphere. The system has both feedforward and feedback paths from the energy and charge conserving dynamical equations (3)–(8).

$$\frac{d}{dt}\left(\frac{1}{2}L_1 I_1^2\right)=\frac{L_1 M}{L_1 L-M^2}(V_{\rm sw}-V)I_1 + \frac{L_1 L}{L_1 L-M^2}(V-V_i)I_1, \tag{7}$$

$$\frac{d}{dt}\left(\frac{1}{2}C_i V_i^2\right)=I_1 V_i-[\Sigma_0+\gamma(I_1 V_i)^{1/2}]V_i^2. \tag{8}$$

The simplest derivation of the ideal part of electrical dynamics follows from the variational (Euler–Lagrange) equations for the action integral over the model current distribution.[3,11] Energy conservation follows from Eqs. (3)–(8), where the total system energy is given by

$$W=\tfrac{1}{2}LI^2-MII_1+\tfrac{1}{2}L_1^2+\tfrac{1}{2}CV^2+\tfrac{1}{2}C_i V_i^2+\tfrac{3}{2}\Omega P. \tag{9}$$

For the detailed definition of the system parameters we must refer the reader to Refs. 2 and 3 due to space limitations. The conservation of electric charge is given in Ref. 3. The conservation of energy and charge then leads to the ''competition'' in the dynamics giving rise to the bifurcations of the system. The energy flows from the solar wind dynamo voltage $V_{\rm sw}$, through WINDMI's feedforward and feedback loops, and is eventually lost from the system due to the ionospheric dissipation and parallel outflow, and is given in Fig. 2. The details of the energy flow through the system are given in Ref. 15.

III. DIMENSION OF ATTRACTORS, SOLAR WIND DRIVING, AND NOISE

Early studies of the correlation dimension, ν, of the auroral AL and AE geomagnetic indices suggested low-dimensional behavior with a correlation dimension of $\nu\approx 3.6$.[16] Following that initial work, Shan *et al.*[17] first raised the question of the electrojet data being colored noise, and Ref. 18 raised the issue of the influence of the solar wind turbulence on these estimates of the electrojet index correlation dimension. Both questions are being investigated with respect to the WINDMI model.

After Shan *et al.*[17] noted that the measured dimension of the electrojet data could be the result of colored noise, the question was studied in detail by a number of authors[19–21] often with contradictory results.[21] Takalo *et al.*,[21] for instance, study the structure function (SF)

$$S=\langle|x(t_i)-x(t_0)|\rangle \tag{10}$$

of the AE index and both the Lorenz attractor and bicolored noise, and reports that the SF of the AE index bears more similarity to the SF of bicolored noise than that of a dynamical system like the Lorenz attractor. However, Pavlos *et al.*[20] study the variance

$$V=\langle|x(t_i)-x(t_0)|^2\rangle \tag{11}$$

and report that the variance of the AE index does not diverge with $(t-t_0)$, as would be expected for colored noise. We obtain results similar to Ref. 20 by considering the variance of a finite subset of the AE record

$$V_s=\langle|x_i-\langle x\rangle|^2\rangle. \tag{12}$$

For colored noise, one would expect the variance of a random subset to be different from that of the entire record, while for a dynamical system the variance of any subset should be the same as that of the entire record. This is because the lowest frequency component of a colored noise signal is determined by the length of the record, while dynamical systems extend over most of their spatial range in any one orbit, and only make close returns on successive orbits. Figure 3(a) for instance shows the variance as a function of the record length for a colored noise signal, while Fig. 3(b) shows the variance of the AL index for the Bargatze dataset. We see that the variance of the AL data does not increase with the length of the record, as would be expected by a colored noise signal. Figure 3(c) shows the variance of the output of the WINDMI model under constant driving as a function of the record length.

The error bars in all three parts of the graph are the standard error of the mean calculated by considering all nonoverlap records of length N (the longest record, at $N=40\,000$ does not have an error bar because it corresponds to only one measurement).

The question of the influence of noise and of the dimensionality of the solar wind on the observed dimension of the AL index was raised by Ref. 18, who used the method of principal value decomposition (singular value decomposition) to reconstruct the coherent part of the geomagnetic indices $[\mathrm{AL}(t), \mathrm{AE}(t)]$, and reject the minute–time scale fluctuations. The resulting reconstructed (filtered) geomagnetic time series show convergence to a correlation dimension $\nu\simeq 2.5$. The influence of noise can be accounted for on the same basis as colored noise. The dimensionality of the dynamical component is exhibited by the lowest frequencies (the repeated returns of the system), while the highest frequencies contain most of the noise (see, for example, Ref. 20). The effect of the dynamical dimension of the solar wind however, is still an open question. Pavlos *et al.*[20] for instance, calculated the dimensionality of the solar wind to be 4.5–4.8 (for the temperature and magnetic field, respectively), while the dimensionality of the AL index was reported to be 3.6 by Ref. 16. Since the magnetosphere is a driven system it is important to question whether the ob-

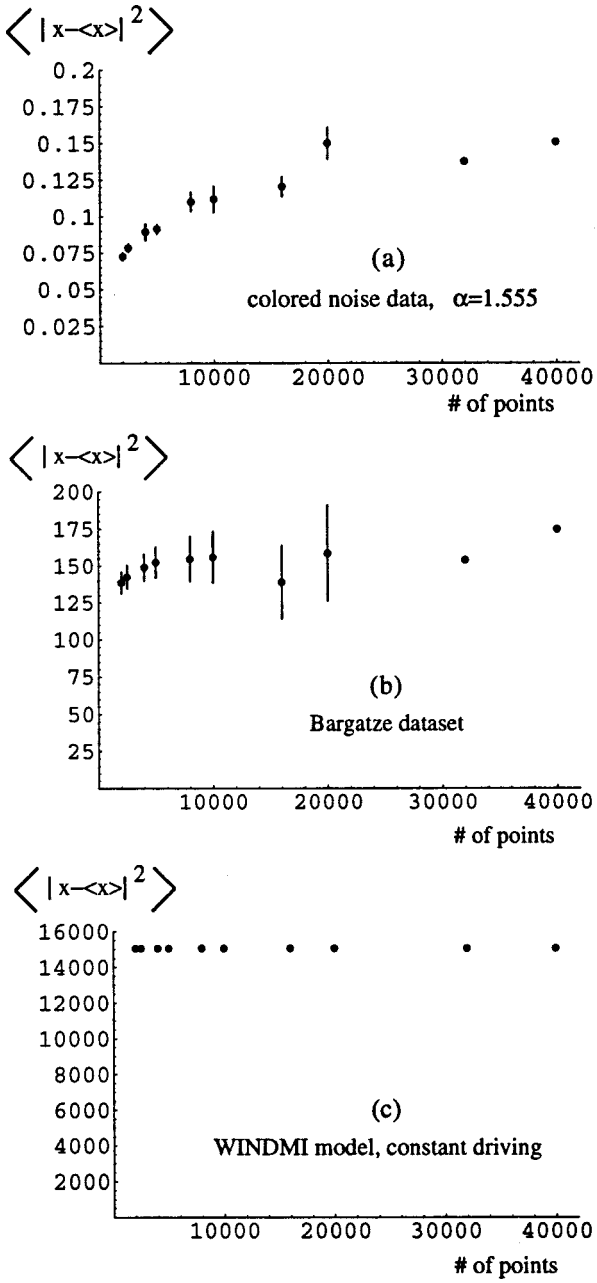

FIG. 3. This graph shows the variance, $V_s=\langle|x_i-\langle x\rangle|^2\rangle$, of a subset of a time series as a function of the length of the subset. (a) shows a colored noise signal, (b) shows the Bargatze dataset, and (c) shows the output of the WINDMI model under constant driving. In all cases the full record is 40 000 points.

served dimensionality of the (driven) AL index is only a reflection of the driver. We are therefore investigating the dimensionality of known chaotic systems driven by another chaotic system. Figure 4, for instance, shows the correlation dimension of the Lorenz system ($d=2.05$) driven by the Rossler system ($d=1.88$). We see that, as expected, for low enough driving we recover the dimensionality of the Lorenz system. As the driver amplitude is increased, however, the driven system exhibits the dimension of a new combined system that is neither the undriven system nor the driver, and finally, for strong enough driving, the dimension of the driver itself. This study has implications for real world systems in which the system of interest cannot be studied except under the influence of its driver, a good example of which is the solar-wind–magnetospheric system.

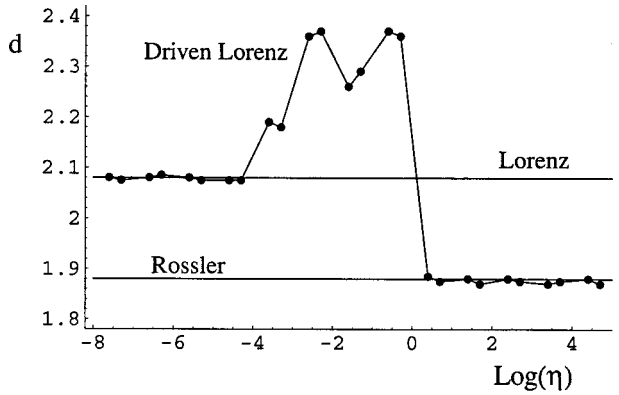

FIG. 4. This graph shows the correlation dimension of a Lorenz system being driven by a Rossler system. For comparison the dimensions of the unperturbed Lorenz and Rossler system are plotted as straight lines. The X axis is the log of the driving parameter, η, normalized to the amplitude of the driven system ($\eta=1$ corresponds to the amplitude of the Rossler data times the unnormalized driving parameter being equal to the amplitude of the Lorenz data). The model shows an example of how the dimensionality of a driven chaotic system ($\nu_L=2.08$) can change to the dimensionality of the driver ($\nu_R=1.88$) for sufficiently strong driving.

IV. BIFURCATION SEQUENCES

The fixed point equation for the WINDMI system yields two roots: one high energy state which is always unstable, and another low-energy ground state root that changes its stability as a function of the system parameters. As the coherent part of the solar-wind electric field varies we track the value of the low-state fixed point in the state phase. Numerical integrations of the system reveal that after the low-state fixed point loses its stability there are (i) limit cycles; (ii) period doubling bifurcations; (iii) a 3-period torus,[22] and (iv) chaotic solutions. The chaotic solutions can occur after a sequence of period doubling bifurcations or after the 3-period solution is destabilized. From a mathematical-physics perspective it is of great interest to determine the sequence of bifurcations and the correlation dimension of the resulting time series. From the point of view of space weather forecasting the tracking of the fixed point with solar wind input is the highest priority, along with a qualitative description of the dynamical excursions about the fixed point. We have made a first study of this behavior. We survey the steady, increasing solar wind input. This type of coherent input is characteristic of magnetic cloud events.

In Fig. 5 we show the bifurcation diagram for the behavior of the cross-tail potential $V(t)$, measured relative to its dimensionless fixed point value V^{FP} with increasing solar wind voltage V_{sw}. We see the period doubling, then the chaotic domain, followed by the inverse bifurcations back to a new high level of steady unloading. Through this sequence of complex dynamical ionospheric electric fields, the fixed points of the ionospheric electric field and current are

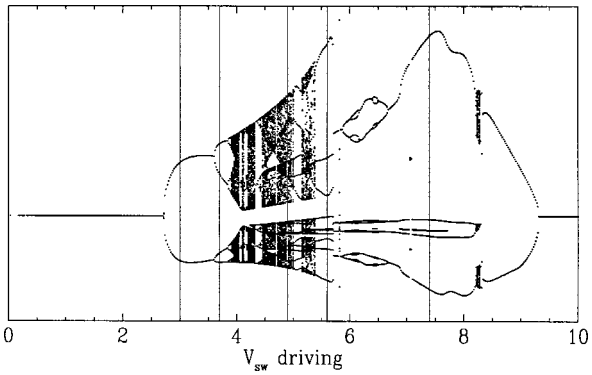

FIG. 5. Comparison of the WINDMI prediction for the ionospheric current with the database westward electrojet index AL(t) for the Bargatze interval 30 with high (>1000 nT) peak disturbances. Note that the geomagnetic index AL(t) is the envelope of signals from a chain of ground-based magnetometers at auroral latitudes and thus is not a true measure of the nightside electrojet current. Generally, the difference is thought to be small for the strong (>1000 nT) auroral disturbances.

$$I_1^{\mathrm{FP}} = \Sigma_i V_{\mathrm{sw}} + \tfrac{1}{2}(\Sigma^{nl})^2 V_{\mathrm{sw}}^3 + \tfrac{1}{2}\Sigma^{nl} V_{\mathrm{sw}}^{3/2}\sqrt{(\Sigma^{nl})^2 V_{\mathrm{sw}}^3 + 4\Sigma_i V_{\mathrm{sw}}}, \qquad V_i^{\mathrm{FP}} = V_{\mathrm{sw}}. \tag{13}$$

At the end of the inverse bifurcations the magnetosphere is in a steady unloading state. In a future work we will give the evidence that this new high level, steady unloading state has the properties associated with magnetic storms.

In Fig. 5 the bifurcation diagram is generated by plotting, for each forcing level on the x-axis the values of the cross-tail potential when the derivative of the cross-tail potential is zero. This includes both the positive and negative turning points (second derivative), so that if one were to plot these linearly versus forcing, the full-scale oscillation of the response to constant driving would be shown by the upper and lower bounds. However, Fig. 5 is not plotted linearly because the full scale variation is much smaller than the value of the fixed point about which it oscillates, and such a plot would be indistinguishable from a plot of the fixed point versus forcing. Instead, the value of the fixed point is subtracted from the values of the turning points, and the result is divided by the fourth power of the fixed point value at that level of forcing. The result shows the period doubling and chaos much more clearly. Increasing forcing, one can see a bifurcation from a stable fixed point to a period one oscillation around $\hat{V}_{\mathrm{sw}}=2.75$, a period doubling at about $\hat{V}_{\mathrm{sw}}=3.6$, and the eventual cascade into chaos. At stronger forcing, there are also some period three and five regions, and the system eventually returns to stability at strong forcing. The details of the nonlinear dynamical properties of the model are given in Ref. 23.

Here we will make the hypothesis from the new finding discovered from the WINDMI model that the magnetic stormlike states lasting for periods of order 100 h and followed by a quiet time without substorms are the final inverse bifurcation of this complex dynamical system. The working

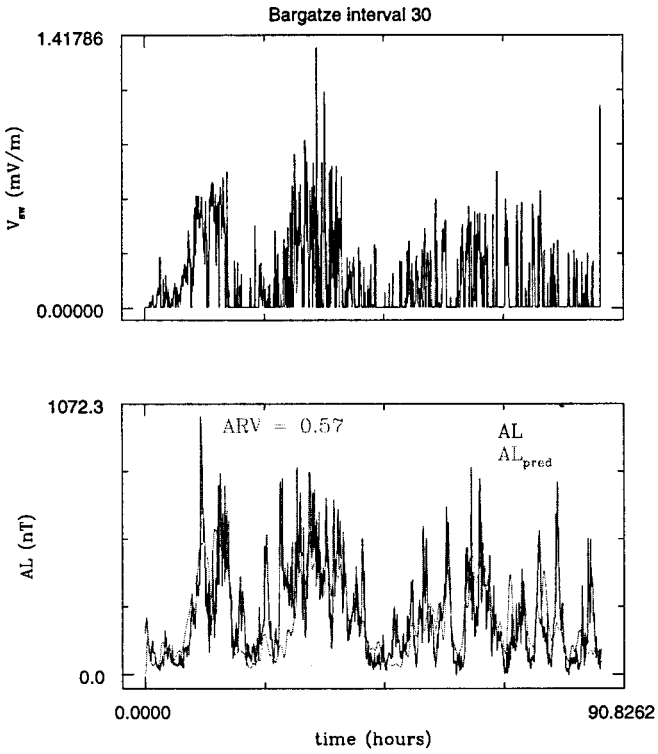

FIG. 6. Bifurcation diagram for the types of attractors given for one particular set of system parameters $\{\mu\}$. The bifurcation parameter (on the x-axis) is the solar-wind driving voltage, V_{sw}. The y axis is a scaled measure of the deviation of the ionospheric potential V (at recorded points where $dV/dt=0$) from the corresponding fixed point value given in Eq. (13).

hypothesis is that these new, high level attractor states are the magnetic storms. The details of this study are given in Ref. 15.

V. INTRINSIC LIMITS OF PREDICTABILITY

In complex dynamical systems the inverse of the maximum Lyapunov exponent ($\lambda_{\max}$) gives a quantitative measure of the limits on predictability. As seen from the bifurcation diagram there are many different regimes $\{\mathbf{X}_i(t_0)\}$ with different values of $\lambda_{\max}$. Here we remark that for a cloud of initial conditions with fractional differences less than 10^{-3} we find that for high level intervals of Bargatze data that there are well-defined predictions up to several tens of hours, after which the trajectories differ qualitatively.

In Fig. 6 we show the performance of the model on one of the highest activity levels in the Bargatze *et al*. database. The system is not using any part of the output in the forecast and is using an optimized set of parameters related to those in Ref. 3 for the interval 20 with moderate levels of geomagnetic activity. For this long (109 h) period is only able to capture about 50% of the actual AL(t) time series as measured by the average relative variance (ARV). For comparison we have recently developed a neural network[24] trained with the high level intervals (21–31) that gives an ARV (neural net)=0.25. We expect to be able to improve the WINDMI ARV significantly, but the nonlinear filter and

neural networks will always have lower ARVs for a given database. It remains to be seen how the comparison with global magnetohydrodynamic (MHD) simulations and real space weather forecasting will compare with WINDMI and its future upgrades.

VI. CONCLUSIONS

Substorms show a wide variety of spatial–temporal forms with multiscale physics clearly evident. Time histories of isolated substorms covered by coordinated data collections from multiple spacecraft and ground based observatories show a clear global coherence of large regions of the nightside magnetosphere coupled with the ionosphere. These properties are consistently given by the six-dimensional WINDMI model that tracks the flow of energy input from the solar wind through the geotail, CPS and the nightside region-1 current loop closing in the auroral oval. Comparisons of the energies given by WINDMI are consistent with those estimated by Ref. 25. Thus, we conclude that WINDMI provides a clear physical model derived from first principle considerations involving a coupling of microscale kinetic physics coupled to large scale MHD behavior for describing the flow of energy through the nightside magnetosphere.

The model needs improvement in its description of competing mechanisms for the bifurcation of the magnetic field leading to the rapid unloading. This would replace the generic rapid unloading switch in the pressure equation [Eq. (5)] with a detailed kinetic theory threshold condition.[26–28] The model also needs to be coupled to an inner magnetosphere system: particularly a description of the injection of the energized CPS ions and electrons into the ring current orbits. This would most likely involve a loss term to the perpendicular flow energy in the plasma sheet [Eq. (4)] as well as a model for ring current injection.

These future generations of the WINDMI model should, we expect, be able to turn the existing idealized model into a powerful, fast forecasting tool. Predictions from VB_s-signals at the Lagrangian L_1 point take a few million floating point operations (FLOP) allowing the construction of ensemble of predictive runs in minutes of real time. In contrast a full global MHD run (see, for example, Ref. 29) will take of order 10^{12} FLOP requiring essentially the entire disturbance propagation time of ~50 min to make a new MHD run. Neural networks and other prediction filters[31] would then seem to be the only serious competing method of making real time forecast.

We point out that such database trained networks have no constraints for energy and charge conservation and may well be unable to model large, rare geomagnetic events. Even for the famous Bargatze dataset we have recently shown that training over the full database seriously degrades performance of a filtered prediction at the highest level of activation.[24] We suggest that nonlinear scientists experienced with driven dissipative systems may find the study of the WINDMI model rewarding.

ACKNOWLEDGMENTS

This work was supported in part by the National Science Foundation Grant No. ATM-97262716, National Aeronautics and Space Administration, NAGW 6198, and by the U.S. Dept. of Energy, Contract No. DE-FG03-96ER-54346.

[1] J. Gleick, *Chaos: Making a New Science* (Viking Penguin, New York, 1988).
[2] W. Horton and I. Doxas, ''A low-dimensional energy conserving state space model for substorm dynamics,'' J. Geophys. Res. **101**, 27223–27237 (1996).
[3] W. Horton and I. Doxas, ''A low-dimensional dynamical model for the solar wind driven geotail-ionosphere system,'' J. Geophys. Res. **103**, 4561–4572 (1998).
[4] W. Horton, M. Pekker, and I. Doxas, ''Magnetic energy storage and the nightside magnetosphere-ionosphere coupling,'' Geophys. Res. Lett. **25**, 4083–4086 (1998).
[5] J. P. Smith, Ph.D. thesis, University of Texas, Austin, 1999, IFSR #863.
[6] L. F. Bargatze, D. N. Baker, R. L. McPherron, and E. W. Hones, ''Magnetospheric response to the IMF: substorms,'' J. Geophys. Res. **90**, 6387 (1985).
[7] C. J. Farrugia *et al*., ''The earth's magnetosphere under continued forcing: Substorm activity during the passage of an interplanetary magnetic cloud,'' J. Geophys. Res. **98**, 7657 (1993).
[8] C. R. Clauer, R. L. McPherron, C. Searls, and M. G. Kivelson, ''Solar wind control of auroral zone geomagnetic activity,'' J. Geophys. Res. **88**, 2123 (1983).
[9] T. Chang, IEEE Trans. Plasma Sci. **20**, 691 (1992), and other authors in this issue.
[10] Y. Kamide *et al*., ''Current understanding of magnetic storms: Storm-substorm relationships,'' J. Geophys. Res. **103**, 17705 (1998).
[11] N. Padhye and W. Horton, ''Alfvén wave particle interaction in finite-dimensional self-consistent field model,'' Phys. Plasmas **6**, 970 (1999).
[12] A. J. Klimas *et al*., ''A nonlinear dynamic analog model of geomagnetic activity,'' J. Geophys. Res. **97**, 12253 (1992).
[13] E. Marsch and C.Y. Tu, in *Proceedings of Solar Wind 7*, edited by E. Marsch and R. Schwenn (Pergamon, Oxford, Goslar, Germany, 1992).
[14] W. Horton, J. V. Hernandez, T. Tajima, and A. Dykhne, ''Fluctuation-dissipation relations for plasmas in strongly inhomogeneous magnetic fields,'' Physica D **21**, 249–259 (1994), and references therein for the fluctuation-dissipation relations.
[15] J. P. Smith, W. Horton, and D. N. Baker (unpublished).
[16] D. V. Vassiliadis, A. S. Sharma, T. E. Estman, and K. Papadopoulos, ''Low-dimensional chaos in magnetospheric activity from AE time series,'' Geophys. Res. Lett. **17**, 1841 (1990).
[17] L. H. Shan, P. Hansen, C. K. Goertz, and R. A. Smith, ''Chaotic appearance of the AE index,'' Geophys. Res. Lett. **18**, 147 (1991).
[18] A. S. Sharma, D. Vassiliadis, and K. Papadopoulos, ''Reconstruction of low-dimensional magnetospheric dynamics by singular spectrum analysis,'' Geophys. Res. Lett. **20**, 335–338 (1993).
[19] D. Prichard and C. P. Price, ''Spurious dimension estimates from geomagnetic time series,'' Geophys. Res. Lett. **19**, 1623 (1992).
[20] G. P. Pavlos *et al*., ''Evidence for strange attractor structures in space plasmas,'' Ann. Geophys. (C.N.R.S.) **10**, 309 (1992).
[21] J. Takalo, J. Timonen, and H. Koskinen, ''Correlation dimension and affinity of AE data and bicolored noise,'' Geophys. Res. Lett. **20**, 1527 (1993).
[22] T. Y. Li and J York, ''Period three orbit implications of chaos,'' J. Am. Math. Month. **82**, 985 (1975).
[23] J. P. Smith, J.-L. Thiffeault, and W. Horton (unpublished).
[24] R. S. Weigel, W. Horton, T. Tajima, and T. Detman, ''Forecasting auroral electrojet activity from solar wind input with neural networks,'' Geophys. Res. Lett. (in press).
[25] D. N. Baker, T. I. Pulkkinen, M. Hesse, and R. L. McPherron, ''A quantitative assessment of energy storage and release in the Earth's magnetotail,'' J. Geophys. Res. **102**, 7159 (1997).
[26] P. L. Pritchett and F. V. Coroniti, ''Interchange and kink modes in the near-Earth plasma sheet and their associated plasma flows,'' Geophys. Res. Lett. **24**, 2925–2928 (1997).

[27]P. L. Pritchett, F. V. Coroniti, and R. Pellat, ''Convection-driven reconnection and the stability of the near-Earth plasma sheet,'' Geophys. Res. Lett. **24**, 873–876 (1997).
[28]A. Roux *et al.*, ''Plasma sheet instability related to the westward traveling surge,'' J. Geophys. Res. **96**, 17697–17714 (1991).
[29]K. Papadopoulos *et al.*, Space Sci. Rev. **71**, 671 (1995).
[30]N. A. Tsyganenko and D. P. Stern, Modeling of the global magnetic field of the large-scale Birkeland current systems, J. Geophys. Res. **101**, 27187–27198 (1996).
[31]D. A. Vassiliadis, A. J. Klimas, D. N. Baker, and D. A. Roberts, A description of solar wind-magnetosphere coupling based on nonlinear filters, J. Geophys. Res. **99**, 3495 (1994).